Unraveling Subunit Cooperativity in Homotetrameric HCN2 Channels

Klaus Benndorf,[†*] Susanne Thon,[†] and Eckhard Schulz[‡]
[†]Institut für Physiologie II, Universitätsklinikum Jena, Friedrich-Schiller-Universität Jena, Jena, Germany; and [‡]Fakultät Elektrotechnik, Fachhochschule Schmalkalden, Schmalkalden, Germany

ABSTRACT In a multimeric receptor protein, the binding of a ligand can modulate the binding of a succeeding ligand. This phenomenon, called cooperativity, is caused by the interaction of the receptor subunits. By using a complex Markovian model and a set of parameters determined previously, we analyzed how the successive binding of four ligands leads to a complex cooperative interaction of the subunits in homotetrameric HCN2 pacemaker channels. The individual steps in the model were characterized by Gibbs free energies for the equilibria and activation energies, specifying the affinity of the binding sites and the transition rates, respectively. Moreover, cooperative free energies were calculated for each binding step in both the closed and the open channel. We show that the cooperativity sequence positive-negative-positive determined for the binding affinity is generated by the combined effect of very different cooperativity sequences determined for the binding and unbinding rates, which are negative-negative-positive and no-negative-no, respectively. It is concluded that in the ligand-induced activation of HCN2 channels, the sequence of cooperativity based on the binding affinity is caused by two even qualitatively different sequences of cooperativity that are based on the rates of ligand binding and unbinding.

INTRODUCTION

Cooperativity can be defined in its broadest sense as a multistep process of basically similar events, in which past events essentially modulate succeeding events by either promoting them (positive cooperativity) or impeding them (negative cooperativity) (1,2). In multimeric receptor proteins, such an event can be the binding of a ligand to a subunit. This binding triggers a change in the interaction of the subunits and in turn leads to a change of the successive ligand binding, thereby modulating activation of the receptor protein. Three mechanisms seem to be possible (3): the binding affinity is the same at all binding sites and is only changed by activation of the receptor; binding affinity is already present from the interaction of the binding domains independent of the receptor state; or it is changed by both receptor activation and interaction of the binding domains.

Ligand-gated ion channels are a big class of multimeric proteins whose activity is controlled by the binding of ligands. They are activated or inhibited by ligands, possibly through either positive cooperativity (e.g., nicotinic acetylcholine receptors (4), CNGA1 channels (5), or P2X2 channels (6)), negative cooperativity (e.g., NMDA receptors (7) or K_{ATP} channels (8)), or positive and negative cooperativity together (e.g., P2X7 receptors (9)). These conclusions were mainly derived from Hill coefficients in concentration-activation relationships. However, a Hill coefficient is physically nonsensical: it only provides a lower limit for the minimum number of ligands involved in the gating (3). Also, a few concentration-binding relationships, obtained with the help of radiolabeled ligands, have been reported to characterize channel activation (nicotinic receptors (10) and GABA receptors (11)), but these Hill coefficients have the same limitations.

More detailed insight into the mechanism of ligand-gated ion channels has been obtained from analyzing time-dependent macroscopic currents, or open probabilities, generated by channels in response to jumps in the ligand concentration by either simulating the currents (e.g., glutamate receptors (12) or nicotinic receptors (13)) or fitting them with Markovian models (e.g., nicotinic receptors (14,15)). Also, these kinds of kinetic analyses are limited by a lack of stringency, and in the case of the fit, the models often have to be oversimplified.

An alternative approach is to extend the analysis to a global fit of multiple traces at the same time (16). At the single-channel level, sophisticated global-fit strategies have been developed for glycine receptors (17,18) and nicotinic receptors (19,20) that have led to Markovian models of formidable complexity, containing up to 18 free parameters. In all these approaches the ligand binding itself could only be measured indirectly. Since sufficiently stringent information is often not available for the modeling strategies, it is useful to make simplifying assumptions, e.g., of an equal affinity at the binding sites or an equal increase of affinity by channel opening at each degree of ligand binding, as used in the famous Monod-Wyman-Changeux (MWC) model (21). However, an interaction of the subunits also can mean that the affinity of the empty binding sites does not change systematically with the degree of ligand binding.

We previously developed a method to measure ligand binding and channel gating simultaneously by combining patch-clamp fluorometry (PCF) (22) with confocal microscopy and using a fluorescence-labeled ligand (23). For CNGA2 channels activated by a fluorescent cGMP, we showed strong negative cooperativity for the second binding

Submitted July 30, 2012, and accepted for publication September 14, 2012.

*Correspondence: Klaus.Benndorf@mti.uni-jena.de

0006-3495/12/11/1860/10 $2.00
http://dx.doi.org/10.1016/j.bpj.2012.09.024

step and strong positive cooperativity for the third binding step. Recently, we analyzed the gating of HCN2 channels by combining confocal PCF with the method of concentration jumps (24), employing as the ligand a fluorescence-labeled cAMP derivative, fcAMP (25). Using global fit of the time courses of ligand binding and channel activation, as well as those of ligand unbinding and channel deactivation, allowed us to determine a Markovian model in great detail. The model contained four binding steps in both the closed and open channels, as well as five closed-open isomerizations. Most remarkably, with respect to the ligand-binding steps, we observed complex cooperativity with a positive-negative-positive sequence. In contrast, the MWC model proved to be inadequate to describe ligand binding and gating (Fig. S1 in the Supporting Material).

In this work, we further study the complex gating of HCN2 channels by analyzing the parameters of our Markovian model. Knowledge of the rate constants in the individual transitions allows us to energetically revisit the term cooperativity, relating it not only to the affinity of the binding sites but also to the rates of binding and unbinding and, moreover, for both the closed and open channels. For the binding steps, three different types of cooperativity are specified and related to the energetics of the closed-open isomerizations at each degree of ligand binding. We show that based on the analysis of rates, the types of cooperativity even qualitatively differ from those based on analysis of equilibrium parameters.

MATERIALS AND METHODS

Determination of the constants

The model considered herein (24), referred to as the C4L-O4L model, contains five closed and five open states, resulting in a network with four cycles (Fig. 1). The equilibrium and rate constants and their errors were determined as described in detail previously (24). In brief, averaged time courses of binding/unbinding and of activation/deactivation, each at 0.075, 0.75, and 7.5 μM fcAMP, were subjected to a global-fit strategy using a modified Levenberg-Marquardt algorithm with 66 data points from each of the six time courses. In each cycle of the model, the parameters were constrained to obey the principle of detailed balance. In the fit, the squares of the deviations at each time and concentration were weighted by the reciprocal values of the respective variances, the χ^2 value was minimized, and the goodness of fit was judged also by the χ^2 value. The calculations were performed with the Eigenvalue method. The data points were shown to be independent. In derived parameters, the mean $\pm$ SE was calculated according to the rules of error propagation and using the respective covariance values.

Calculation of cooperative free energies for microscopic equilibria

The equilibrium association constant for the first binding step in the C4L-O4L model is K_{AC1} (Table S1). Because it is plausible to assume that the homotetrameric empty channel contains four equivalent binding sites, the equilibrium association constant for one of these subunits should be ${}^1K_{AC1} = K_{AC1}/4$. Assuming now that all binding steps employ binding sites equivalent to those in the empty channel, this generates theoretical equilibrium association constants ($K_{ACx,th}$) for the first through fourth binding steps in the homotetrameric channel of $K_{AC1,th} = 4 \times {}^1K_{AC1} = K_{AC1}$, $K_{AC2,th} = 3/2 \times {}^1K_{AC1}$, $K_{AC3,th} = 2/3 \times {}^1K_{AC1}$, and $K_{AC4,th} = 1/4 \times {}^1K_{AC1}$, using the stoichiometric factors for an independent binding. For these theoretical equilibrium association constants of each binding step of the whole channel, the theoretical free energies $\Delta G^{th}(C_{x-1} \leftrightarrow C_x)$ ($x = 1\ldots4$) were calculated according to Eq. 1, corresponding to a channel with no interaction between the binding sites, i.e., no cooperativity. All differences between the free energies determined by the global fit with the C4L-O4L model and these theoretical free energies should therefore specify cooperative free energies for the individual binding steps of the whole channel, $\Delta\Delta G_{coop}(C_{x-1} \leftrightarrow C_x) = \Delta G(C_{x-1} \leftrightarrow C_x) - \Delta G^{th}(C_{x-1} \leftrightarrow C_x)$ ($x = 1\ldots4$). The same derivation holds for the open channel, $\Delta\Delta G_{coop}(O_{x-1} \leftrightarrow O_x) = \Delta G(O_{x-1} \leftrightarrow O_x) - \Delta G^{th}(O_{x-1} \leftrightarrow O_x)$ ($x = 1\ldots4$). All energy values are listed in Table 1.

For the closed-open isomerizations, a cooperative free energy among the subunits was calculated by using Eq. 1 with $Y = E_x$ (Table 1 and Table S1) at each degree of ligand binding with respect to the free energy of the

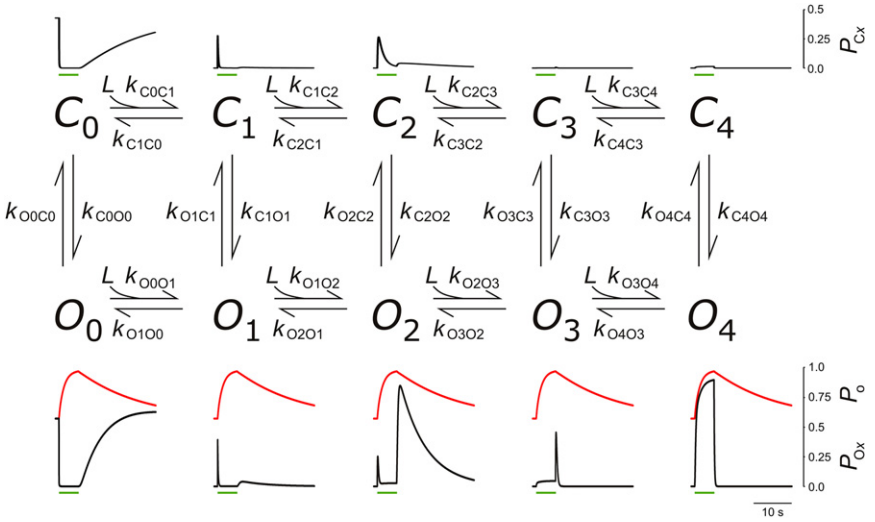

FIGURE 1 Scheme of the C4L-O4L model. The C4L-O4L model was used to describe the additional activation-and-deactivation time course of HCN2 channels after preactivation by a voltage step to −130 mV. The model contains five closed (C_x) and five open states (O_x; x = 0…4), with four ligand-binding steps in both the closed and open channel, as well as five closed-open isomerizations. The rate constants for the ligand-induced activation were determined previously by subjecting the time courses of ligand binding and activation gating to a global fit (24). The values of the rate constants are listed in Table S1. $k_{O3C3} = k_{O4C4}$ were set to 20 s^{-1}, resulting in $k_{C3O3} = k_{C4O4} = 1.3 \times 10^3$ s^{-1}. With these values, χ^2 reached the minimum. Below and above the states, the time courses of their population (expressed as open probabilities, P_{Cx} and P_{Ox}; $x = 0\ldots4$) are indicated for a fcAMP jump from zero to 7.5 μM and back to zero. The time of exposure to fcAMP is indicated by green bars. The sum of all states adds to unity at each time. P_o denotes the time course of the total open probability (ΣP_{Ox}, $x = 0\ldots4$), drawn in red above each individual time course of P_{Ox}.

TABLE 1 Energies of the transitions in the C4L-O4L model

Transition	$\Delta G^{\ddagger}$	$\Delta\Delta G^{\ddagger}_{coop}$	Equilibrium	ΔG	$\Delta\Delta G_{coop}$
$C_0 \rightarrow C_1$*	62.70 ± 0.19	0	$C_0 \leftrightarrow C_1$*	-5.81 ± 0.06	0
$C_1 \rightarrow C_0$	68.51 ± 0.20	0			
$C_1 \rightarrow C_2$*	67.21 ± 0.11	3.81 ± 0.25	$C_1 \leftrightarrow C_2$*	-10.25 ± 0.08	-6.83 ± 0.13
$C_2 \rightarrow C_1$	77.47 ± 0.12	10.64 ± 0.27			
$C_2 \rightarrow C_3$*	72.43 ± 0.05	8.04 ± 0.19	$C_2 \leftrightarrow C_3$*	5.95 ± 0.14	7.40 ± 0.16
$C_3 \rightarrow C_2$	66.48 ± 0.15	0.64 ± 0.26			
$C_3 \rightarrow C_4$*	59.21 ± 0.35	−6.86 ± 0.41	$C_3 \leftrightarrow C_4$*	−7.27 ± 0.21	−8.20 ± 0.20
$C_4 \rightarrow C_3$	66.48 ± 0.15	1.34 ± 0.26			
$O_0 \rightarrow O_1$*	61.60 ± 0.16	0	$O_0 \leftrightarrow O_1$*	−7.85 ± 0.03	0
$O_1 \rightarrow O_0$	69.45 ± 0.17	0			
$O_1 \rightarrow O_2$*	65.91 ± 0.06	3.61 ± 0.16	$O_1 \leftrightarrow O_2$*	−10.48 ± 0.06	−5.02 ± 0.09
$O_2 \rightarrow O_1$	76.39 ± 0.02	8.63 ± 0.17			
$O_2 \rightarrow O_3$*	66.70 ± 0.21	3.41 ± 0.28	$O_2 \leftrightarrow O_3$*	−1.29 ± 0.17	2.20 ± 0.17
$O_3 \rightarrow O_2$	67.98 ± 0.19	1.21 ± 0.28			
$O_3 \rightarrow O_4$*	59.21 ± 0.35	−5.76 ± 0.39	$O_3 \leftrightarrow O_4$*	−7.27 ± 0.21	−6.17 ± 0.21
$O_4 \rightarrow O_3$	66.48 ± 0.15	0.41 ± 0.22			
$C_0 \rightarrow O_0$	79.56 ± 0.22	0	$C_0 \leftrightarrow O_0$	−0.70	0
$O_0 \rightarrow C_0$	80.26 ± 0.22	0			
$C_1 \rightarrow O_1$	69.78 ± 0.19	−9.78 ± 0.29	$C_1 \leftrightarrow O_1$	−2.73 ± 0.04	−2.03 ± 0.04
$O_1 \rightarrow C_1$	72.51 ± 0.21	−7.75 ± 0.29			
$C_2 \rightarrow O_2$	81.81 ± 0.84	2.25 ± 0.93	$C_2 \leftrightarrow O_2$	−2.96 ± 0.04	−2.26 ± 0.04
$O_2 \rightarrow C_2$	84.77 ± 0.86	4.51 ± 0.95			
$C_3 \rightarrow O_3$	58.83	−20.73	$C_3 \leftrightarrow O_3$	−10.19	−9.49
$O_3 \rightarrow C_3$	69.01	−11.25			
$C_4 \rightarrow O_4$	58.83	−20.73	$C_4 \leftrightarrow O_4$	−10.19	−9.49
$O_4 \rightarrow C_4$	69.01	−11.25			

ΔG and $\Delta G^{\ddagger}$ were computed according to Eqs. 1 and 2, respectively, using the equilibrium or rate constants given in Table S1. The concentration-dependent free energies (*) were calculated for 7.5 μM fcAMP. Energies at other fcAMP concentrations (x, in μM) can be obtained by adding ($-RT\ln(x/7.5\ \mu M)$). $\Delta\Delta G_{coop}$ and $\Delta\Delta G^{\ddagger}_{coop}$ were computed as described in Materials and Methods. They are independent of the fcAMP concentration. $\Delta G^{\ddagger}(O_3 \rightarrow C_3) = \Delta G^{\ddagger}(O_4 \rightarrow C_4)$ was computed with $k_{O3C3} = k_{O4C4} = 3\ s^{-1}$, which is 10× the estimated lower border (see Table S1). Accordingly, $\Delta G^{\ddagger}(C_3 \rightarrow O_3) = \Delta G^{\ddagger}(C_4 \rightarrow O_4)$ was computed with $k_{C3O3} = k_{C4O4} = 2.0 \times 10^2\ s^{-1}$. All energies are given in kJ M^{-1}. The errors, denoted as the mean ± SE, are based on the variances in the fit (main diagonal of the covariance matrix), obeying the principles of error propagation.

nonliganded channel ($C_0 \leftrightarrow O_0$) by $\Delta\Delta G_{coop}(C_x \leftrightarrow O_x) = \Delta G(C_x \leftrightarrow O_x) - \Delta G(C_0 \leftrightarrow O_0)$ ($x = 1\ldots4$).

Calculation of cooperative activation energies

Cooperative activation energies for all microscopic rates of binding and unbinding ($\Delta\Delta G^{\ddagger}_{coop}$; Table 1) were computed as follows. For the binding of ligand 1 to the closed empty channel, it is assumed that the four binding sites are equivalent, i.e., the binding rate for one of these subunits should be ${}^1k_{C0C1} = k_{C0C1}/4$. Assuming that all binding steps employ binding sites equivalent to those in the empty channel, this generates theoretical rate constants for the first through fourth binding steps in the whole homotetrameric channel of $k_{C0C1,th} = 4 \times {}^1k_{C0C1} = k_{C0C1}$, $k_{C1C2,th} = 3 \times {}^1k_{C1C2}$, $k_{C2C3,th} = 2 \times {}^1k_{C2C3}$, and $k_{C3C4,th} = 1 \times {}^1k_{C3C4}$, using the stoichiometric factors for an independent binding. For these theoretical rate constants of each binding step in the whole channel, the theoretical activation energies, $\Delta G^{\ddagger th}(C_{x-1} \rightarrow C_x)$ ($x = 1\ldots4$), were calculated according to Eq. 2. This approach is valid for a theoretical channel with no cooperativity between the binding sites. All differences between $\Delta G^{\ddagger}(C_{x-1} \rightarrow C_x)$, determined with the C4L-O4L model (compare to Fig. 4 *A*), and $\Delta G^{\ddagger th}(C_{x-1} \rightarrow C_x)$ should therefore specify the cooperative activation energy for the individual binding steps in the whole channel, $\Delta\Delta G^{\ddagger}_{coop}(C_{x-1} \rightarrow C_x) = \Delta G^{\ddagger}(C_{x-1} \rightarrow C_x) - \Delta G^{\ddagger th}(C_{x-1} \rightarrow C_x)$ ($x = 1\ldots4$). $\Delta\Delta G^{\ddagger}_{coop}(C_{x-1} \rightarrow C_x)$ does not depend on the ligand concentration.

For the unbinding transitions also, we referred all activation energies to the unbinding of ligand 1. The unbinding rate for the one liganded subunit in the monoliganded channel is given by ${}^1k_{C1C0} = k_{C1C0}$. Assuming that all unbinding steps employ binding sites equivalent to those in the monoliganded channel, this generates theoretical rate constants for the unbinding of ligands 4–1 in the whole homotetrameric channel of $k_{C4C3,th} = 4 \times {}^1k_{C1C0}$, $k_{C3C2,th} = 3 \times {}^1k_{C1C0}$, $k_{C2C1,th} = 2 \times {}^1k_{C1C0}$, and $k_{C1C0,th} = 1 \times {}^1k_{C1C0} = k_{C1C0}$, using the stoichiometric factors for an independent unbinding. For these theoretical rate constants of each unbinding step in the whole channel, the theoretical activation energies, $\Delta G^{\ddagger th}(C_x \rightarrow C_{x-1})$ ($x = 1\ldots4$) were calculated according to Eq. 2, again specifying a theoretical channel with no cooperativity between the binding sites. All differences between $\Delta G^{\ddagger}(C_x \rightarrow C_{x-1})$, determined with the C4L-O4L model (compare Fig. 4 *A*), and $\Delta G^{\ddagger th}(C_x \rightarrow C_{x-1})$ should therefore specify cooperative activation energies for the individual unbinding steps in the whole channel, $\Delta\Delta G^{\ddagger}_{coop}(C_x \rightarrow C_{x-1}) = \Delta G^{\ddagger}(C_x \rightarrow C_{x-1}) - \Delta G^{\ddagger th}(C_x \rightarrow C_{x-1})$ ($x = 1\ldots4$). The same derivations apply for the binding and unbinding transitions of the open channel, resulting in $\Delta\Delta G^{\ddagger}_{coop}(O_{x-1} \rightarrow O_x) = \Delta G^{\ddagger}(O_{x-1} \rightarrow O_x) - \Delta G^{\ddagger th}(O_{x-1} \rightarrow O_x)$ and $\Delta\Delta G^{\ddagger}_{coop}(O_x \rightarrow O_{x-1}) = \Delta G^{\ddagger}(O_x \rightarrow O_{x-1}) - \Delta G^{\ddagger th}(O_x \rightarrow O_{x-1})$, respectively ($x = 1\ldots4$). For the opening and closing transitions, the respective activation energies were related to those of the nonliganded channel, yielding $\Delta\Delta G^{\ddagger}_{coop}(C_x \rightarrow O_x) = \Delta G^{\ddagger}(C_x \rightarrow O_x) - \Delta G^{\ddagger}(C_0 \rightarrow O_0)$ and $\Delta\Delta G^{\ddagger}_{coop}(O_x \rightarrow C_x) = \Delta G^{\ddagger}(O_x \rightarrow C_x) - \Delta G^{\ddagger}(O_0 \rightarrow C_0)$ ($x = 1\ldots4$).

RESULTS

The C4L-O4L model

The C4L-O4L model is shown in Fig. 1. The values of the rate constants are provided in Table S1. They were obtained

by a global fit to multiple time courses of ligand binding and activation gating induced by concentration jumps of fcAMP to HCN2 channels preactivated by a voltage step to −130 mV (24). At this voltage, voltage-dependent activation was nearly maximal and the binding of fcAMP evoked a robust extra activation of the channels. Though the structure of the C4L-O4L model shares similarity with the MWC model (21), the C4L-O4L model is fundamentally different from the MWC model in that it does not assume the same affinity at the binding sites. The C4L-O4L model thus allows for both positive and negative cooperativity with respect to the binding affinity. Moreover, the availability of a complete set of rate constants enabled us to consider the population of each individual state as a function of time. As reported previously, the total open probability is dominated by open states with either zero, two, or four ligands bound, but not by states with one or three ligands bound, which are only transiently populated in the sense of intermediates (24). Related to the affinity at the binding sites this suggests positive cooperativity between the first and the second, as well as the third and fourth, binding steps. Conversely, the stabilized double-liganded state suggests pronounced negative cooperativity between the second and third binding steps.

Cooperativity based on the binding affinity

Cooperativity is regularly attributed to the binding affinity of a receptor. To gain mechanistic insight into conformational changes of a multimeric receptor, we considered the microscopic affinity of the individual binding sites, which is independent of subsequent conformational changes (3). The microscopic affinity at a binding site can be quantified by the equilibrium association constant, K_A, specifying the binding of a single ligand to an empty receptor, thereby forming a ligand-receptor complex. Conformational changes proceeding at the binding site when the ligand binds are included in K_A. The major conformational change associated with channel opening and closing is described by the equilibrium constant for the closed-open isomerization, E.

Using the values of the equilibrium constants for our C4L-O4L model (Table S1), we calculated the Gibbs free energy, ΔG, for all transitions according to

$$\Delta G = -RT \ln(Y), \quad (1)$$

where R and T are the molar gas constant and the temperature. Y is either K_{ACx} or K_{AOx}, ($x = 1\ldots4$) times the actual ligand concentration, or E_x (x = 0…4).

Fig. 2 *A* shows a plot of these free energies for the four binding steps at three very different ligand concentrations and for both the closed and open channel. In the diagram below (Fig. 2 *B*), the free energies for the closed-open isomerizations are shown. All energies are free energies

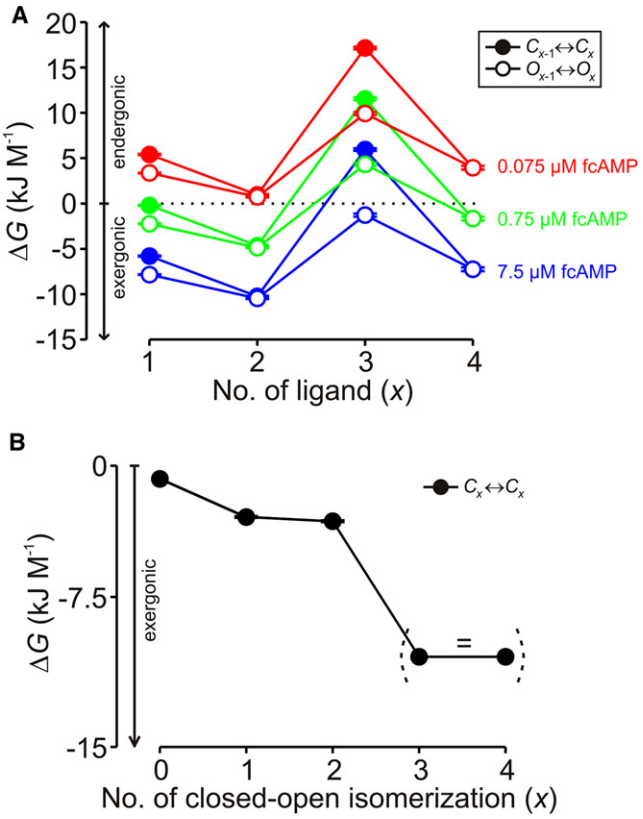

FIGURE 2 Gibbs free energies in ligand-induced activation. The Gibbs free energies (ΔG) were calculated from the equilibrium constants in Table S1 according to Eq. 1. (*A*) Gibbs free energies for the binding steps at three ligand concentrations. ΔG moves in the direction from endergonic to exergonic in proportion to an increased ligand concentration. At all concentrations, and in both the closed and open channel, the second binding step causes the minimum and the third binding step the maximum ΔG value. (*B*). Gibbs free energies for the closed-open isomerizations. All values are exergonic. $\Delta G(C_3 \leftrightarrow O_3)$ and $\Delta G(C_4 \leftrightarrow O_4)$ are equal, because E_3 and E_4 were set equal in the fit.

for the whole activated channel. Together these diagrams provide the following results. 1), At all ligand concentrations, the second binding step has the smallest ΔG value, whereas the third binding step has the largest ΔG value. This mirrors the mentioned positive cooperativity for the second and fourth binding steps and the negative cooperativity for the third binding step. 2), Increasing the ligand concentration from 0.075 μM to 7.5 μM fcAMP shifts the relationship from the endergonic range to the exergonic range. At 7.5 μM fcAMP, only $\Delta G(C_2 \leftrightarrow C_3)$ remains endergonic. 3), All closed-open isomerizations are exergonic but to different degrees: $\Delta G(C_0 \leftrightarrow O_0)$ is only slightly exergonic, $\Delta G(C_1 \leftrightarrow O_1)$ and $\Delta G(C_2 \leftrightarrow O_2)$ are intermediately exergonic and similarly large, whereas $\Delta G(C_3 \leftrightarrow O_3)$ and $\Delta G(C_4 \leftrightarrow O_4)$ are much more exergonic. This suggests that the successive binding of four ligands evokes only two levels of activation (24).

Next we calculated the cooperative free energy for the whole channel arising from the subunit interaction at each

degree of ligand binding (Materials and Methods). Notably, these cooperative free energies are independent of the ligand concentration. By introducing these cooperative free energies into the binding steps of the C4L-O4L model, we could illustrate how the subunit cooperativity modulates the ligand binding in homotetrameric HCN2 channels (Fig. 3). These results substantiate the pronounced positive cooperativity ($\Delta\Delta G_{coop}<0$) for the second and fourth binding steps and the pronounced negative cooperativity ($\Delta\Delta G_{coop}>0$) for the third binding step, and this is not only with respect to their previous steps, but also with respect to the first binding step, generated by empty and, presumably, equivalent subunits.

Also for the closed-open isomerizations, a cooperative free energy among the subunits was calculated at each degree of ligand binding with respect to that of $C_0 \leftrightarrow O_0$ (Materials and Methods). Inclusion of these cooperative free energies in the C4L-O4L model allowed us to relate them both to each other and to the cooperative free energies of the binding steps (Fig. 3). Two major conclusions can be drawn: 1), the strongest effect of the closed-open transition on $\Delta\Delta G_{coop}(C_{x-1} \leftrightarrow C_x)$ and $\Delta\Delta G_{coop}(O_{x-1} \leftrightarrow O_x)$ is to decrease that of the third binding step; and 2), when the endergonic third binding step ($\Delta G_{coop}(C_2 \leftrightarrow C_3)$ or $\Delta G_{coop}(O_2 \leftrightarrow O_3)$) is past, all subsequent free energies ($\Delta\Delta G_{coop}(C_3 \leftrightarrow O_3)$, $\Delta\Delta G_{coop}(C_4 \leftrightarrow O_4)$, $\Delta\Delta G_{coop}(C_3 \leftrightarrow C_4)$, $\Delta\Delta G_{coop}(O_3 \leftrightarrow O_4)$) are substantially exergonic. This has two effects: the population of the fully liganded open state, O_4, is strongly promoted and the energetically obstructed binding of the third ligand becomes possible, in analogy to the much simpler delCastillo-Katz mechanism (3).

Cooperativity based on rates differs qualitatively from that based on equilibria

All of the above considerations on cooperativity were performed for conditions of microscopic equilibria. Because any chemical equilibrium is generated by two opposed reactions, neither a microscopic affinity nor an equilibrium of a closed-open isomerization specifies a single physical process; rather, they each consist of a combination of two processes. Referring this to the above definition of cooperativity as a "multistep process of basically similar events, in which past events significantly modulate succeeding events," we considered in detail the activation energies of the individual transitions and their relations to each other. Such an approach should provide more detailed information about the phenomenon of subunit cooperativity than any analysis based on parameters describing microscopic equilibria.

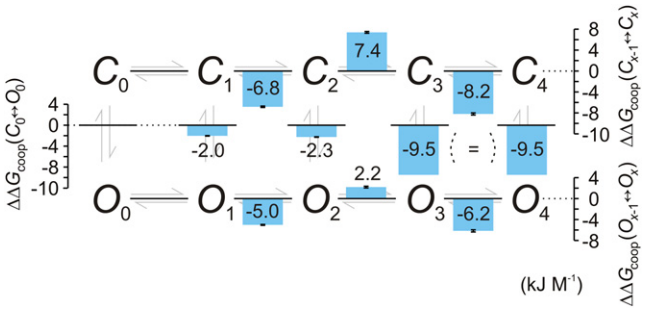

FIGURE 3 Cooperative free energies of the transitions in the C4L-O4L model. The cooperative free energies for the binding steps, $\Delta\Delta G_{coop}$ $(C_{x-1} \leftrightarrow C_x)$ and $\Delta\Delta G_{coop}(O_{x-1} \leftrightarrow O_x)$ $(x = 1\ldots4)$, and the closed-open isomerizations, $\Delta\Delta G_{coop}(C_x \leftrightarrow O_x)$ $(x = 0\ldots4)$, were obtained as described in the text. The values are attributed to the transitions as bars and numbers in kJ M^{-1}. All energy values are related to the energy values for the first binding step, in both the closed and open channel, and the first closed-open isomerization, respectively, resulting in zero values for these transitions (*black lines*).

According to the transition-state theory (26), a rate constant of a reaction, k, corresponds to the Gibbs free energy of forming one mole of the activated complex in this reaction, $\Delta G^{\ddagger}$, by

$$\Delta G^{\ddagger} = -RT \ln\left(\frac{kh}{\kappa k_B T}\right), \quad (2)$$

where R is the molar gas constant, T the temperature, h the Planck constant, and k_B the Boltzmann constant. The transmission coefficient, κ, was set to unity (27). As is customary, $\Delta G^{\ddagger}$ will be referred to here as activation energy. The $\Delta G^{\ddagger}$ values for all binding and unbinding processes in the closed channel and the open channel are plotted in Fig. 4, *A* and *B*, respectively. Concerning the binding steps, the $\Delta G^{\ddagger}$ values for ligands 2 and 3 are larger than those for ligands 1 and 4, in both the closed and open channel. The main difference between the closed and open channel is that $\Delta G^{\ddagger}(C_2 \rightarrow C_3)$ is maximal alone (Fig. 4 *A*, *green curves*), whereas $\Delta G^{\ddagger}(O_2 \rightarrow O_3)$ is as large as $\Delta G^{\ddagger}(O_1 \rightarrow O_2)$ (Fig. 4 *B*, *red curves*). In contrast to the $\Delta G^{\ddagger}$ values for binding, the $\Delta G^{\ddagger}$ values for unbinding develop a pronounced maximum for ligand 2 (Fig. 4 *A*, *orange curve*, and Fig. 4 *B*, *blue curve*), whereas $\Delta G^{\ddagger}$ is as low for ligand 3 as for ligand 4 (set equal in the case of the closed channel).

Fig. 4, *A* and *B*, also shows that the effect of increasing the fcAMP concentration is a shift of the binding relationships to a lower level (Fig. 4, *A* and *B*, *dark green* and *dark red curves*, respectively), thereby differentially changing the $\Delta G^{\ddagger}$ relation between binding and unbinding for ligands 2 and 3. For both the closed and open channel, the $\Delta G^{\ddagger}$ value for the binding of ligand 2 approximately balances that for unbinding even at the low concentration of 0.075 μM fcAMP (Fig. 4 *A*, *ligand 2*, *light green* and *orange points*). In contrast, for ligand 3, the $\Delta G^{\ddagger}$ value for binding remains larger than that for unbinding at all concentrations in the closed channel (Fig. 4 *A*, *ligand 3*, *green* and *orange points*) and at the two lower concentrations in the open channel (Fig. 4 *B*, *ligand 3*, *light* and *medium red points* versus *blue point*). Only in the open channel at the high concentration of 7.5 μM fcAMP is the $\Delta G^{\ddagger}$ value for binding close to that for unbinding (Fig. 4 *B*, *ligand 3*, *dark red* and *blue*

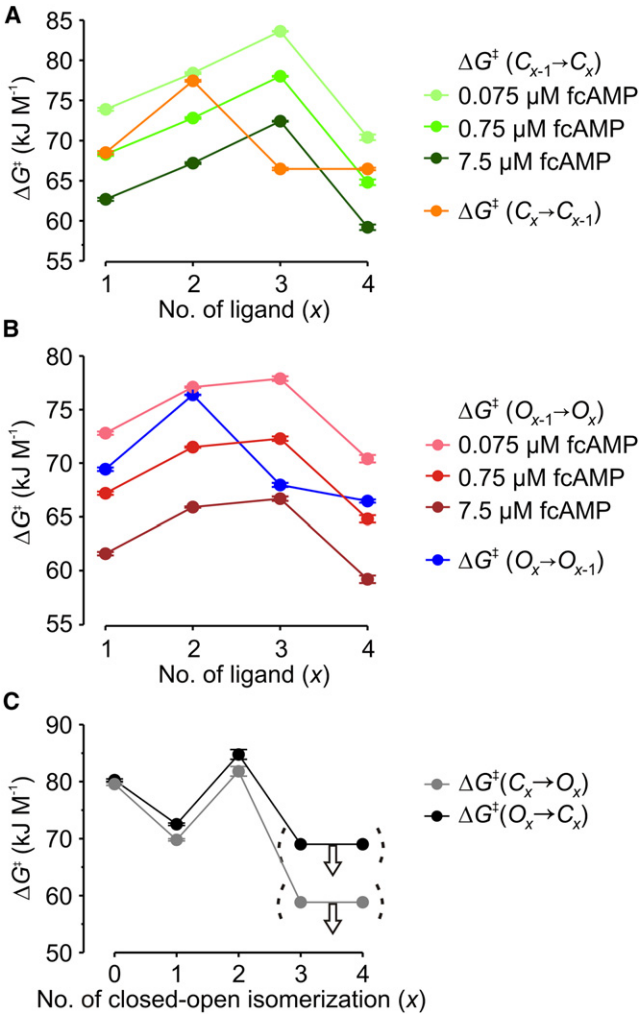

FIGURE 4 Activation energies. (*A*) Activation energies ($\Delta G^{\ddagger}$) for the binding rates at three fcAMP concentrations and the unbinding rates in the closed channel. ($x = 1\ldots4$). (*B*) Same as *A*, but for the open channel. (*C*) Activation energies of the closed-open isomerizations ($x = 0\ldots4$). The dotted parentheses and the arrow indicate that the rate constants with three and four ligands bound were set equal and are a lower estimate. All values of $\Delta G^{\ddagger}$ were calculated according to Eq. 2.

points). In contrast, for ligands 1 and 4, an increase of the fcAMP concentration from 0.075 to 7.5 μM moves the energy balance from unbinding-dominated to binding-dominated.

We next considered the $\Delta G^{\ddagger}$ values corresponding to the rates in the closed-open isomerizations (Fig. 4 *C*). Comparing the $\Delta G^{\ddagger}$ values for $C_0 \leftrightarrow O_0$, $C_1 \leftrightarrow O_1$, and $C_2 \leftrightarrow O_2$, it can be seen that the value of 70 kJ M^{-1} for $C_1 \leftrightarrow O_1$ is notably smaller than the values of 80 and 83 kJ M^{-1} for $C_0 \leftrightarrow O_0$ and $C_2 \leftrightarrow O_2$, respectively. This means that $C_1 \leftrightarrow O_1$ equilibrates 30–100 times faster than $C_0 \leftrightarrow O_0$ and $C_2 \leftrightarrow O_2$. Using the estimated lower borders for the rate constants determining $C_3 \leftrightarrow O_3$ and $C_4 \leftrightarrow O_4$ ($k_{O3C3} = k_{O4C4} > 0.3\ s^{-1}$, $k_{C3O3} = k_{C4O4} > 2.0\ s^{-1}$; Table S1), the resulting $\Delta G^{\ddagger}$ values indicate that the closed-open isomerizations $C_3 \leftrightarrow O_3$ and $C_4 \leftrightarrow O_4$ equilibrate at least as rapidly as does $C_1 \leftrightarrow O_1$. This leads to the conclusion that the states with zero and two ligands bound are taut, allowing only very slow closed-open transitions, whereas states with one, three, and four ligands bound are flexible (relaxed), allowing much faster closed-open transitions.

In analogy to $\Delta\Delta G_{coop}$ for the microscopic equilibria, we calculated cooperative activation energies for all binding transitions in the C4L-O4L model, $\Delta\Delta G^{\ddagger}_{coop}$, specifying that part of the activation energy that arises from cooperative effects with respect to the first binding step (Materials and Methods). For the unbinding transitions we also related all considerations to the unbinding of ligand no. 1, being aware that this is not the first but the last of the four unbinding steps. The reason for this approach was that we could assume no cooperativity when a ligand unbinds from a monoliganded channel. All energy values correspond to the whole channel (Materials and Methods).

Plotting $\Delta\Delta G^{\ddagger}_{coop}(C_{x-1} \rightarrow C_x)$ and $\Delta\Delta G^{\ddagger}_{coop}(C_x \rightarrow C_{x-1})$, as well as $\Delta\Delta G^{\ddagger}_{coop}(O_{x-1} \rightarrow O_x)$ and $\Delta\Delta G^{\ddagger}_{coop}(O_x \rightarrow O_{x-1})$, as a function of the ligand number (Fig. 5 *A*) reveals the following results. 1), The $\Delta\Delta G^{\ddagger}_{coop}$ values are generally much smaller than the $\Delta G^{\ddagger}$ values (Fig. 4 *A*) but are in the range of the free energies determined for the microscopic equilibria (Fig. 3) (2). In the binding reaction, $\Delta\Delta G^{\ddagger}_{coop}$ is

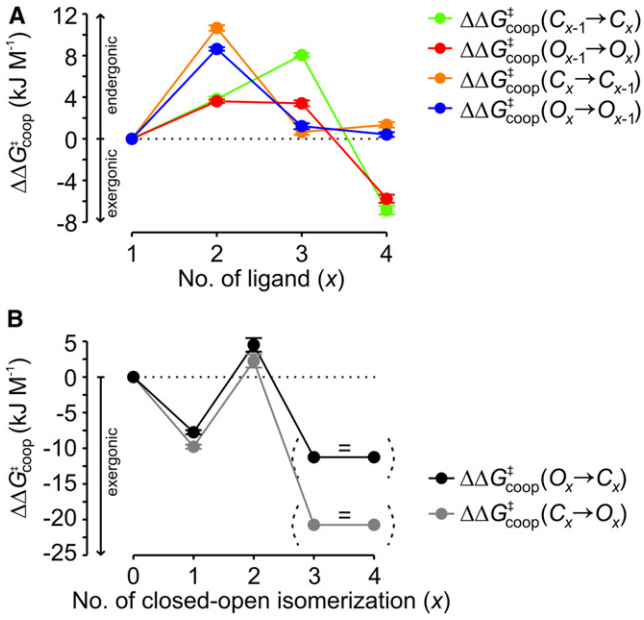

FIGURE 5 Cooperative activation energies. (*A*) Cooperative activation energies of the binding and unbinding reactions in the closed and open channel, $\Delta\Delta G^{\ddagger}_{coop}$, as a function of the number of the ligand (x). The main effect of channel opening is to decrease $\Delta\Delta G^{\ddagger}_{coop}$ of the third binding step. For unbinding, $\Delta\Delta G^{\ddagger}_{coop}$ is similar in the closed and open channel at all degrees of ligand binding. (*B*) Cooperative activation energies, $\Delta\Delta G^{\ddagger}_{coop}$, of the closed-open and open-closed isomerizations as a function of the number of ligands bound (x). The dotted parentheses and the equal sign indicate that the rate constants with three and four ligands bound were set equal.

positive for ligands 2 and 3 and negative for ligand 4 (Fig. 5 *A*, *red* and *green curves*). The most pronounced effect of the closed-open isomerization is that $\Delta\Delta G^{\ddagger}_{coop}$ for ligand 3 is selectively reduced from 8.0 to 3.4 kJ M^{-1} (3). In the unbinding reaction, a pronounced positive $\Delta\Delta G^{\ddagger}_{coop}$ of ~10 kJ M^{-1} is only associated with ligand 2, whereas ligands 4 and 3 generate only small values (Fig. 5 *A*, *blue* and *orange curves*). These results further underline as a remarkable feature of the channel the fact that the binding of ligand 3 and the unbinding of ligand 2 are the steps that have the greatest impact in the ligand-induced gating.

Also for the closed-open isomerizations, at each degree of ligand binding, cooperative activation energies were calculated with respect to the activation energies of the unliganded channel (Materials and Methods). A plot of the resulting values shows that $\Delta\Delta G^{\ddagger}_{coop}(C_x \rightarrow O_x)$ is generally shifted in the exergonic direction with respect to $\Delta\Delta G^{\ddagger}_{coop}(O_0 \rightarrow C_0)$ and that in the diliganded channel there is an endergonic peak for both the opening and closing reactions (Fig. 5 *B*). The preponderance of exergonic energies, in particular when ligands 3 and 4 are bound, shows that the free energy gained by ligand binding is directed to a substantial extent into the reduction of $\Delta\Delta G^{\ddagger}_{coop}$ in both channel opening and closing.

DISCUSSION

Cooperativity by binding affinity

When the term cooperativity is used for receptor proteins, it is generally related to the binding affinity for ligands or to the macroscopic apparent affinity, as determined by functional assays. For the HCN2 channel, we previously identified a complex type of cooperativity by determining microscopic equilibria. Relating the equilibrium association constants of binding steps 2, 3, and 4 to those of their previous steps, 1, 2, and 3, respectively, the cooperativity sequence was positive-negative-positive (24). In this study, we translated the equilibrium association constants to Gibbs free energies by using Eq. 1. To specify cooperative free energies, $\Delta\Delta G_{coop}$, for binding steps 2, 3, and 4, we related their free energies to that of step 1, when the channel is empty and any ligand-induced cooperativity can be excluded. The procedure is described in Materials and Methods. Fig. 6 *A* illustrates in a color-coded fashion the energetics of the cooperativity for the binding affinity. The sequence of the $\Delta\Delta G_{coop}$ values provides the same type of positive-negative-positive cooperativity (Fig. 6 *A*, *brackets*) as obtained by relating the steps to their respective previous steps. Note that all $\Delta\Delta G_{coop}$ values denote free energies for the whole channel and not for a single subunit. We favored this idea because in the cases of three or two empty subunits, it is still unknown how these energies are distributed among the empty subunits. Despite this lack of knowledge, this approach allowed us to easily demonstrate the complex

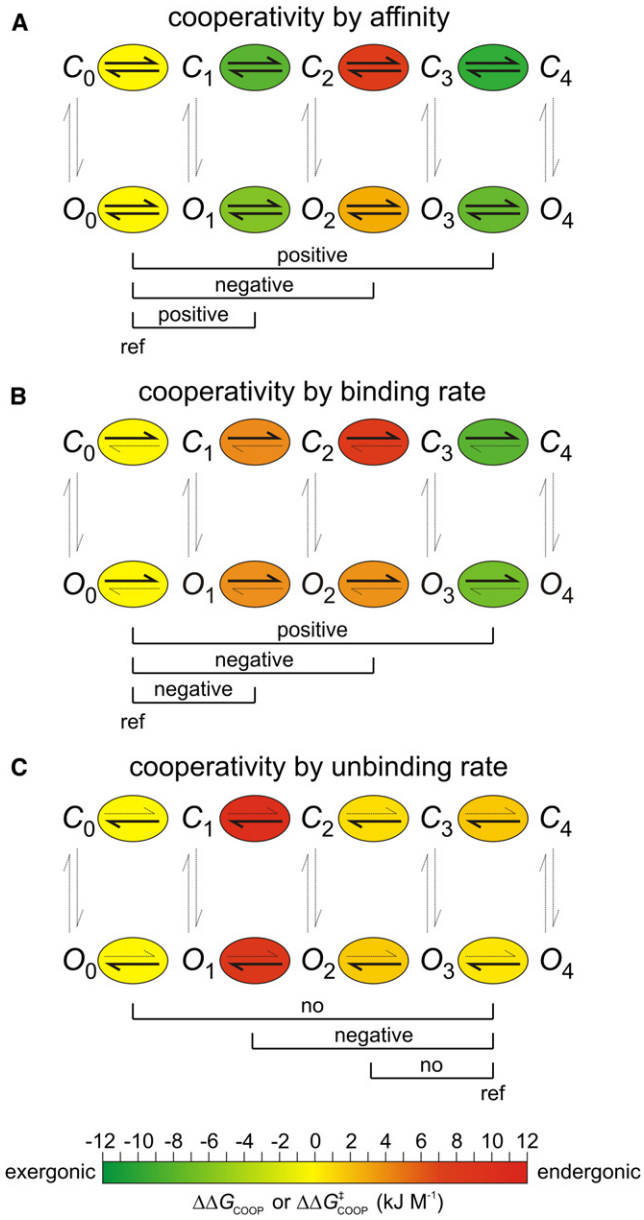

FIGURE 6 Illustration of the different types of cooperativity. The scheme of the C4L-O4L model corresponds to that in Fig. 1. The four binding steps in the closed and open channel are energetically labeled by colored circles according to the scale below the figure. (*A*) Cooperativity by affinity. The colors denote $\Delta\Delta G_{coop}$. The brackets indicate the sequence of cooperativity if binding steps 2, 3, and 4 are related to binding step 1, where $\Delta\Delta G_{coop}$ was set to zero. *ref*, reference step. (*B*) Cooperativity by binding rate. The colors denote $\Delta\Delta G^{\ddagger}_{coop}$. The brackets indicate the sequence of cooperativity if the binding rates for ligands 2, 3, and 4 are related to the binding rate of ligand 1, for which $\Delta\Delta G^{\ddagger}_{coop}$ was set to zero. (*C*) Cooperativity by unbinding rate. The colors denote $\Delta\Delta G^{\ddagger}_{coop}$. The brackets indicate the sequence of cooperativity if the unbinding rates for ligands 1, 2, and 3 are related to the unbinding rate of ligand 4, for which $\Delta\Delta G^{\ddagger}_{coop}$ was set to zero. For further explanation see text.

type of cooperativity within the channel: activation seems to be operated by functional dimers (24), based on two observations: 1), the first and second ligands evoke only

moderate activation, whereas the third ligand generates full activation; and 2), the two steps with positive cooperativity are separated by a step with negative cooperativity. Since our knowledge about the structure of the HCN2 channel is at present only poor, interpreting our functional results in terms of structure remains speculative.

Note that the cooperativity by the binding affinity differs from that in related CNGA2 channels insofar as in CNGA2 channels the second, but not the third, binding step had a much lower binding affinity than the others (23). However, any comparison between the results in CNGA2 channels and the results in HCN2 channels presented here should be performed with caution due to the facts that CNGA2 channels were not preactivated by voltage and that the models used were different from that used here.

Cooperativity by binding rates

Our strategy of measuring ligand binding and activation gating in parallel enabled us to consider also the activation energies ($\Delta G^{\ddagger}$, Fig. 4, *A–C*), and the cooperative activation energies ($\Delta\Delta G^{\ddagger}_{coop}$, Fig. 5. *A* and *B*) underlying the individual equilibria. For the binding and unbinding reactions, $\Delta\Delta G^{\ddagger}_{coop}$ was obtained by relating the $\Delta G^{\ddagger}$ value to a theoretical free energy, assuming that an empty subunit always works as the first subunit binding a ligand. For the closed channel, the result is that the binding of ligand 3 is the most endergonic, whereas that of ligand 4 is the most exergonic (Fig. 5 *A*, *green curve*). The major effect of channel opening is very specific: It reduces the large endergonic level for the binding of ligand 3 to <50%. If related to the first ligand binding to the empty channel, the cooperativity sequence based on the binding rate is negative-negative-positive for both the closed and open channel (Fig. 6 *B*).

For the unbinding rates, $\Delta\Delta G^{\ddagger}_{coop}$ was obtained by relating the $\Delta G^{\ddagger}$ value to a theoretical free energy, assuming that each liganded subunit unbinds a ligand as does the liganded subunit in the monoliganded channel. Because $\Delta\Delta G^{\ddagger}_{coop}$ for unbinding of ligand 4 was close to $\Delta\Delta G^{\ddagger}_{coop}$ for unbinding of ligand 1, our conclusions are also valid when relating all energies directly to the first unbinding of ligand 4, for both the closed and open channel. The sequence of $\Delta\Delta G^{\ddagger}_{coop}$ for the unbinding reaction is noticeably different from that for the binding reaction: $\Delta\Delta G^{\ddagger}_{coop}$ is close to zero for ligands 4, 3, and 1, whereas a large endergonic level has to be passed for the unbinding of ligand 2. Starting from the fully liganded channel, this results in a cooperativity sequence of no-negative-no (Fig. 6 *C*). Again, this effect is similar in the closed and open channel.

According to Eyring's rate theory, the free energy between any states 1 and 2, ΔG_{12}, is given by the difference between the respective activation energies, $\Delta G^{\ddagger}_1$ and $\Delta G^{\ddagger}_2$. This applies also for $\Delta\Delta G_{coop}$. Hence, Fig. 6, *B* and C, directly illustrate how the cooperativity sequence by affinity (Fig. 6 *A*) results from very different cooperativity sequences for the binding and unbinding of the ligand. This leads to two remarkable results: 1), the endergonic $\Delta\Delta G_{coop}$ step for ligand 3 in Fig. 6 *A* (*red*) is caused by the binding reaction alone; and 2), the nature of the two exergonic $\Delta\Delta G_{coop}$ steps in Fig. 6 *A* (*green*) is unequal: for ligand 2, binding is endergonic and unbinding is even more endergonic, whereas for ligand 4, the exergonic unbinding dominates $\Delta\Delta G_{coop}$.

These results indicate that the subunit interactions strongly modulate the energetics of the binding and unbinding rates. In general, a binding rate can be modulated by a changed diffusional access for a ligand to the binding site or by a changed free energy of the actual conformational changes at the binding site associated with the binding. Modulation of the unbinding rate is primarily thought to be mediated by the respective initial conformational changes. However, a modulated diffusion of an unbound ligand would change the rate of rebinding of the ligand and would thus also lead to an apparent modulation of the unbinding. Our results do not allow us to distinguish between these processes.

Coupling between cooperative ligand binding and channel opening

It is remarkable that the second ligand does not lead to a noticeable change of the cooperative free energy for the closed-open isomerization ($\Delta\Delta G_{coop}(C_2 \leftrightarrow O_2) = -2.96$ kJ M^{-1} versus $\Delta\Delta G_{coop}(C_1 \leftrightarrow O_1) = -2.73$ kJ M^{-1}; Fig. 3). The exergonic cooperative free energies for the second binding step, $\Delta\Delta G_{coop}(C_1 \leftrightarrow C_2)$ and $\Delta\Delta G_{coop}(O_1 \leftrightarrow O_2)$, are apparently stored in the protein outside the pore. If the closed-open isomerization is the only principal conformational change, one may speculate that this energy storage proceeds in the intracellular complex of the four cyclic nucleotide binding domains (28). It is possible that this free energy is then used to skip the endergonic barrier of the third binding step.

Another important point arises when relating the third binding step to the closed-open isomerization: $\Delta\Delta G_{coop}$ $(C_2 \leftrightarrow C_3)$ is substantially more endergonic than $\Delta\Delta G_{coop}$ $(O_2 \leftrightarrow O_3)$ (Fig. 3), whereas $\Delta\Delta G_{coop}(C_3 \leftrightarrow O_3)$ is substantially more exergonic than $\Delta\Delta G_{coop}(C_2 \leftrightarrow O_2)$ and, moreover, all subsequent free energies, $\Delta\Delta G_{coop}(C_3 \leftrightarrow C_4)$, $\Delta\Delta G_{coop}(C_4 \leftrightarrow O_4)$, $\Delta\Delta G_{coop}(O_3 \leftrightarrow O_4)$, are also substantially exergonic. This strongly promotes the energetically obstructed binding of ligand 3 in both the closed and open channel, as demonstrated previously for the simpler del-Castillo-Katz mechanism consisting of one binding reaction and one closed-open isomerization (3). This is a good example of how understanding the energetic coupling within a complex Markovian model requires knowledge about as many steps as possible.

Understanding cooperativity needs steric and functional information

If relating the outcome of our approach to the state of knowledge available for oxygen binding to the tetrameric hemoglobin, probably the best studied cooperative mechanism in any multimeric protein (for a review, see Perutz et al. (29)), there are two major differences: First, hemoglobin has been crystallized in different functional states and an enormous amount of information on steric relationships between the subunits has been elaborated, whereas for HCN2 channels only the cyclic nucleotide binding domain (28) has been successfully crystallized so far. Second, a detailed kinetic analysis of the subunit action, as performed previously for HCN2 channels (24), is not available for hemoglobin. The reason for this lack of knowledge concerning hemoglobin is that the binding of oxygen is very rapid, most likely in the submicrosecond time range (for a review, see Cui and Karplus (30)). This is much faster than the binding of fcAMP considered herein, and it complicates any analysis severely. However, one should be aware that measurement of oxygen binding to hemoglobin is done by methods that record actual conformational changes of hemoglobin and not the binding itself, i.e., the kinetics of oxygen binding cannot be measured directly. In contrast, the binding to and activation of HCN2 channels are very slow, and these two entities were even measured independently. Only this combination of data provided the exceptional determinateness of the model parameters and thus the presumption for the analysis presented here. Great progress for a further understanding of the HNC2 channel gating can be expected when our data are related to structural data derived from crystals, which are, however, not available at present.

CONCLUSIONS

In this study, we specified for homotetrameric HCN2 channels how the cooperativity of the subunits based on the binding affinity can be reduced to two sequences based on rates: the cooperativity sequence positive-negative-positive for the binding affinity is caused by the two very different cooperativity sequences negative-negative-positive and no-negative-no for the ligand binding and unbinding rates, respectively. When relating cooperativity to physical processes, a rate is a more elementary process than an equilibrium constant. Therefore, the two cooperativity sequences defined by the rates and the amount of the respective activation energies provide, to the best of our knowledge, a new perspective for considering cooperativity between subunits.

When speculating about the functional role of the cooperativity sequence positive-negative-positive in HCN2 channels, and the underlying highly endergonic barrier in binding step 3, there is a range of low ligand concentrations, in which more subtle regulation is performed that involves only two subunits, and a range of high ligand concentrations, in which a reserve can be added to evoke stronger effects.

SUPPORTING MATERIAL

One figure, one table, and supporting references are available at http://www.biophysj.org/biophysj/supplemental/S0006-3495(12)01061-2.

The authors thank T. Schwabe, A. Schweinitz, V. Nache, R. Schmauder, J. Kusch, and G. Ehrlich for comments on the manuscript. K. Benndorf generated the hypotheses, designed the figures, and wrote the article. K. Benndorf and E. Schulz performed the analyses. S. Thon prepared the figures. E. Schulz and S. Thon commented on the manuscript.

This work was supported by a grant from the Deutsche Forschungsgemeinschaft to K.B.

REFERENCES

1. Neet, K. E. 1995. Cooperativity in enzyme function: equilibrium and kinetic aspects. *Methods Enzymol.* 249:519–567.
2. Maconochie, D. J., and D. E. Knight. 1992. Markov modelling of ensemble current relaxations: bovine adrenal nicotinic receptor currents analysed. *J. Physiol.* 454:155–182.
3. Colquhoun, D. 1998. Binding, gating, affinity and efficacy: the interpretation of structure-activity relationships for agonists and of the effects of mutating receptors. *Br. J. Pharmacol.* 125:924–947.
4. Sine, S. M., and P. Taylor. 1980. The relationship between agonist occupation and the permeability response of the cholinergic receptor revealed by bound cobra α-toxin. *J. Biol. Chem.* 255:10144–10156.
5. Kaupp, U. B., T. Niidome, …, S. Numa. 1989. Primary structure and functional expression from complementary DNA of the rod photoreceptor cyclic GMP-gated channel. *Nature.* 342:762–766.
6. Ding, S., and F. Sachs. 2002. Evidence for non-independent gating of P2X2 receptors expressed in *Xenopus* oocytes. *BMC Neurosci.* 3:17.
7. Regalado, M. P., A. Villarroel, and J. Lerma. 2001. Intersubunit cooperativity in the NMDA receptor. *Neuron.* 32:1085–1096.
8. Hehl, S., and B. Neumcke. 1993. Negative cooperativity may explain flat concentration-response curves of ATP-sensitive potassium channels. *Eur. Biophys. J.* 22:1–4.
9. Michel, A. D., L. J. Chambers, …, I. P. Chessell. 2007. Direct labelling of the human P2X7 receptor and identification of positive and negative cooperativity of binding. *Br. J. Pharmacol.* 151:103–114.
10. Grutter, T., L. Prado de Carvalho, …, J. P. Changeux. 2003. An H-bond between two residues from different loops of the acetylcholine binding site contributes to the activation mechanism of nicotinic receptors. *EMBO J.* 22:1990–2003.
11. Chang, Y., and D. S. Weiss. 1999. Channel opening locks agonist onto the GABAC receptor. *Nat. Neurosci.* 2:219–225.
12. Standley, C., T. M. Norris, …, P. N. Usherwood. 1993. Gating kinetics of the quisqualate-sensitive glutamate receptor of locust muscle studied using agonist concentration jumps and computer simulations. *Biophys. J.* 65:1379–1386.
13. Franke, C., H. Hatt, …, J. Dudel. 1991. Kinetic constants of the acetylcholine (ACh) receptor reaction deduced from the rise in open probability after steps in ACh concentration. *Biophys. J.* 60:1008–1016.
14. Maconochie, D. J., and D. E. Knight. 1992. A study of the bovine adrenal chromaffin nicotinic receptor using patch clamp and concentration-jump techniques. *J. Physiol.* 454:129–153.
15. Milescu, L. S., G. Akk, and F. Sachs. 2005. Maximum likelihood estimation of ion channel kinetics from macroscopic currents. *Biophys. J.* 88:2494–2515.

16. Nache, V., E. Schulz, …, K. Benndorf. 2005. Activation of olfactory-type cyclic nucleotide-gated channels is highly cooperative. *J. Physiol.* 569:91–102.

17. Burzomato, V., M. Beato, …, L. G. Sivilotti. 2004. Single-channel behavior of heteromeric $\alpha 1\beta$ glycine receptors: an attempt to detect a conformational change before the channel opens. *J. Neurosci.* 24:10924–10940.

18. Beato, M., P. J. Groot-Kormelink, …, L. G. Sivilotti. 2004. The activation mechanism of $\alpha 1$ homomeric glycine receptors. *J. Neurosci.* 24:895–906.

19. Lee, W. Y., and S. M. Sine. 2004. Invariant aspartic acid in muscle nicotinic receptor contributes selectively to the kinetics of agonist binding. *J. Gen. Physiol.* 124:555–567.

20. Lape, R., D. Colquhoun, and L. G. Sivilotti. 2008. On the nature of partial agonism in the nicotinic receptor superfamily. *Nature.* 454:722–727.

21. Monod, J., J. Wyman, and J. P. Changeux. 1965. On the nature of allosteric transitions: a plausible model. *J. Mol. Biol.* 12:88–118.

22. Zheng, J., and W. N. Zagotta. 2000. Gating rearrangements in cyclic nucleotide-gated channels revealed by patch-clamp fluorometry. *Neuron.* 28:369–374.

23. Biskup, C., J. Kusch, …, K. Benndorf. 2007. Relating ligand binding to activation gating in CNGA2 channels. *Nature.* 446:440–443.

24. Kusch, J., S. Thon, …, K. Benndorf. 2012. How subunits cooperate in cAMP-induced activation of homotetrameric HCN2 channels. *Nat. Chem. Biol.* 8:162–169.

25. Kusch, J., C. Biskup, …, K. Benndorf. 2010. Interdependence of receptor activation and ligand binding in HCN2 pacemaker channels. *Neuron.* 67:75–85.

26. Glasstone, S., K. J. Laidler, and H. Eyring. 1941. The Theory of Rate Processes. McGraw-Hill, New York.

27. Hille, B. 1992. Ionic Channels of Excitable Membranes. Sinauer Associates, Sunderland, MA.

28. Zagotta, W. N., N. B. Olivier, …, E. Gouaux. 2003. Structural basis for modulation and agonist specificity of HCN pacemaker channels. *Nature.* 425:200–205.

29. Perutz, M. F., A. J. Wilkinson, …, G. G. Dodson. 1998. The stereochemical mechanism of the cooperative effects in hemoglobin revisited. *Annu. Rev. Biophys. Biomol. Struct.* 27:1–34.

30. Cui, Q., and M. Karplus. 2008. Allostery and cooperativity revisited. *Protein Sci.* 17:1295–1307.